The EMBO Journal (2008) 27, 1017–1028 | © 2008 European Molecular Biology Organization | All Rights Reserved 0261-4189/08
www.embojournal.org

THE EMBO JOURNAL

Liver-specific deletion of histone deacetylase 3 disrupts metabolic transcriptional networks

Sarah K Knutson[1], Brenda J Chyla[1,5], Joseph M Amann[1,2], Srividya Bhaskara[1], Stacey S Huppert[3] and Scott W Hiebert[1,4,*]

[1]Department of Biochemistry, Vanderbilt University School of Medicine, Nashville, TN, USA, [2]Department of Cancer Biology, Vanderbilt University School of Medicine, Nashville, TN, USA, [3]Department of Cell and Developmental Biology, Vanderbilt University School of Medicine, Nashville, TN, USA and [4]Vanderbilt-Ingram Cancer Center, Vanderbilt University School of Medicine, Nashville, TN, USA

Histone deacetylase 3 (Hdac3) is an enzymatic component of transcriptional repression complexes recruited by the nuclear hormone receptors. Inactivation of *Hdac3* in cancer cell lines triggered apoptosis, and removal of *Hdac3* in the germ line of mice caused embryonic lethality. Therefore, we deleted *Hdac3* in the postnatal mouse liver. These mice developed hepatomegaly, which was the result of hepatocyte hypertrophy, and these morphological changes coincided with significant imbalances between carbohydrate and lipid metabolism. Loss of *Hdac3* triggered changes in gene expression consistent with inactivation of repression mediated by nuclear hormone receptors. Loss of *Hdac3* also increased the levels of *Pparγ2*, and treatment of these mice with a Pparγ antagonist partially reversed the lipid accumulation in the liver. In addition, gene expression analysis identified mammalian target of rapamycin signalling as being activated after deletion of *Hdac3*, and inhibition by rapamycin affected the accumulation of neutral lipids in *Hdac3*-null livers. Thus, Hdac3 regulates metabolism through multiple signalling pathways in the liver, and deletion of *Hdac3* disrupts normal metabolic homeostasis.
The EMBO Journal (2008) **27,** 1017–1028. doi:10.1038/emboj.2008.51; Published online 20 March 2008
Subject Categories: signal transduction; cellular metabolism
Keywords: chromatin; *Hdac3*; histone acetylation; metabolism

Introduction

Histone deacetylases (HDACs) are classified based on sequence similarity to yeast homologues. Class I HDACs are most similar to yeast Rpd3 and are ubiquitously expressed in many tissues. These enzymes localize primarily to the nucleus and include HDAC 1, 2, 3, and 8. Class II HDACs, which include HDACs 4–7 and 9–11, are related to yeast Hda1 and are expressed in a more tissue-specific manner (de Ruijter *et al*, 2003). Although the putative catalytic domain of class II HDACs is highly homologous to that of class I enzymes, the vertebrate class IIa HDACs (4, 5, 7, and 9) have little intrinsic enzymatic activity, but associate with HDAC3 (Fischle *et al*, 2002; Gallinari *et al*, 2007; Lahm *et al*, 2007). Sirtuins (Sir) are a third class of HDACs, homologous to the yeast Sir2 enzyme, and differ from the first two classes of HDACs in their requirement for NAD^+ for both deacetylase and ADP-ribosylation activities (Gartenberg, 2000; Imai *et al*, 2000).

Gene deletion studies have begun to define the individual physiological roles of class I HDACs. Targeted deletion of *Hdac1* in mice led to embryonic lethality by E10.5, due to proliferation defects, and these defects were also found in cultured embryonic stem cells (Lagger *et al*, 2002; Zupkovitz *et al*, 2006). Inactivation of *Hdac2* in mice resulted in a low percentage of lethality during embryogenesis, but almost half of *Hdac2*-null pups died within a month after birth due to a defect in heart development. *Hdac2*-null mice that survived to a later age had an apparent proliferation defect in the heart tissue and failed to respond normally to hypertrophic induction (Trivedi *et al*, 2007). These genetic models demonstrate the importance of understanding the function of individual HDACs, as well as the tissue-specific requirements for each enzyme.

HDAC3 is an enzymatic component of the nuclear receptor co-repressor complexes that contain N-CoR (nuclear hormone co-repressor) and SMRT (silencing mediator for retinoid and thyroid receptors), which are recruited by nuclear hormone receptors to regulate transcription in the absence of hormone (Li *et al*, 2000; Guenther *et al*, 2001; Yoon *et al*, 2003). Thus, HDAC3 may be required for the normal physiological action of many nuclear hormone receptors and is the critical catalytic component when nuclear hormone receptor functions are disrupted in cancer. For example, the retinoic acid receptor is disrupted by the t(15;17) in acute promyelocytic leukaemia (Alcalay *et al*, 1991) and the action of HDAC3 may be required for leukaemogenesis (Grignani *et al*, 1998; Guidez *et al*, 1998; He *et al*, 1998; Lin *et al*, 1998). Similarly, other leukaemia-related factors such as the t(12;21) and t(8;21) fusion proteins recruit HDAC3, suggesting that this enzyme might be a key therapeutic target in paediatric B-cell acute lymphocytic leukaemia and acute myeloid leukaemia (Chakrabarti and Nucifora, 1999; Fenrick *et al*, 1999, 2000; Guidez *et al*, 2000; Amann *et al*, 2001; Wang and Hiebert, 2001). Indeed, both natural and synthetic histone deacetylase inhibitors (HDIs) are being tested clinically as anticancer agents for the treatment of leukaemia and a variety of solid tumours (Santini *et al*, 2007).

Disruption of *HDAC3* function in cell lines, by either gene deletion or RNAi in tumour cell lines, suggested that HDAC3 was required for maintaining cell viability (Takami and Nakayama, 2000; Glaser *et al*, 2003; Li *et al*, 2006). By

*Corresponding author. Department of Biochemistry, Vanderbilt University School of Medicine, 512 Preston Research Building, 23rd and Pierce Avenue, Nashville, TN 37232, USA.
Tel.: +1 615 936 3582; Fax: +1 615 936 1790;
E-mail: scott.hiebert@vanderbilt.edu
[5]Present address: Abbott Laboratories, Abbott Park, IL, USA

Received: 5 February 2008; accepted: 25 February 2008; published online: 20 March 2008

contrast, primary cells treated with HDIs arrested cell cycle progression, but were more resistant to apoptosis (Papeleu *et al*, 2003). Germline deletion of *Hdac3* triggered early embryonic lethality (Bhaskara *et al*, 2008); therefore, we genetically engineered mice to conditionally delete *Hdac3* in the liver using transgenic mice expressing the interferon-inducible *Mx1*-Cre recombinase (*Mx1-Cre*) or the liver-specific *albumin-Cre* recombinase (*Alb-Cre*). Although there was no dramatic increase in either apoptosis or proliferation due to the initial loss of *Hdac3*, the liver became enlarged over time, which appeared to be due to hepatocyte hypertrophy. In addition, genes that regulate lipid and cholesterol biosynthesis were de-repressed, which in turn resulted in a dramatic increase in both liver and serum levels of triglycerides and cholesterol. Many of these genes are controlled by nuclear hormone receptors, such as peroxisome proliferator-activated receptor gamma (PPARγ) and thyroid hormone receptor (THR), which utilize N-CoR or SMRT and Hdac3 to repress transcription. Multiple signalling pathways contribute to the abnormal metabolic phenotype, as demonstrated by inhibition of Pparγ or mammalian target of rapamycin (mTOR) *in vivo*. Thus, *Hdac3* is required for regulating liver metabolic homeostasis.

Results

Liver-specific deletion of Hdac3 results in organ hypertrophy

Deletion of *Hdac3* in the germ line caused early embryonic lethality (Bhaskara *et al*, 2008). Therefore, to understand the physiological role of *Hdac3* in adult tissue homeostasis, we conditionally deleted *Hdac3* using Cre recombinase-expressing transgenic mice and a 'floxed' allele of *Hdac3* (Supplementary Figure S1). Initially, *Hdac3* heterozygous (+/−) and floxed (fl/+) mice were crossbred with transgenic *Mx1-Cre* mice. To generate tissue-specific heterozygous (*Mx1-Cre*; $Hdac3^{fl/+}$, hereafter referred to as $Mx{:}Hdac3^{fl/+}$) or null (*Mx1-Cre*; $Hdac3^{fl/-}$, hereafter referred to as $Mx{:}Hdac3^{fl/-}$) mice, *Mx1-Cre* expression was stimulated by injecting synthetic double-stranded RNA (polyinosinic-polycytidylic acid (pIpC)) to induce interferon (Kuhn *et al*, 1995). Two days after the final injection of pIpC, RNA was extracted from the liver tissue of $Mx{:}Hdac3^{fl/-}$ mice and analysed by RT–PCR to confirm inactivation of *Hdac3* (Figure 1A). Nuclear lysates from liver samples demonstrated a dramatic decrease in Hdac3 levels in $Mx{:}Hdac3^{fl/-}$ mice (Figure 1B). Two weeks after the final pIpC injection, an increase in liver size and weight of up to two-fold was noted in $Mx{:}Hdac^{fl/-}$ mice (Figure 1C). Histological analysis of $Mx{:}Hdac3^{fl/-}$ livers revealed little change within 2 days of the last injection, but there was a gradual increase in a mosaic pattern of hypertrophic hepatocytes with grainy cytoplasm, which peaked within 2 weeks of the last pIpC injection (Figure 1C).

To complement the analysis with the *Mx1-Cre* model and to avoid possible side effects of interferon signalling affecting liver function, we crossbred $Hdac3^{fl/fl}$ and $Hdac3^{+/-}$ mice with mice expressing Cre recombinase under the control of the *albumin* promoter (*Alb-Cre*) to generate heterozygous (*Alb-Cre*; $Hdac3^{fl/+}$, hereafter referred to as $Alb{:}Hdac3^{fl/+}$) and null (*Alb-Cre*; $Hdac3^{fl/-}$, hereafter referred to as $Alb{:}Hdac3^{fl/-}$) offspring. *Alb-Cre* is expressed in parenchymal liver cells, resulting in roughly 40% recombination in hepatocytes at birth and almost complete recombination by 2 weeks after birth (Postic *et al*, 1999). Although *Hdac3* is required for cell viability *in vitro*, $Alb{:}Hdac3^{fl/-}$ mice were viable, even with observable decreases in *Hdac3* mRNA and protein levels occurring as early as postnatal day 4 (P4; data not shown). Recombination was confirmed by PCR to detect the floxed and null alleles (data not shown). Western blot analysis indicated that Hdac3 levels were dramatically decreased 10 days after birth and were undetectable by P17 in $Alb{:}Hdac3^{fl/-}$ mice (Figure 2A). Western blot and RT–PCR

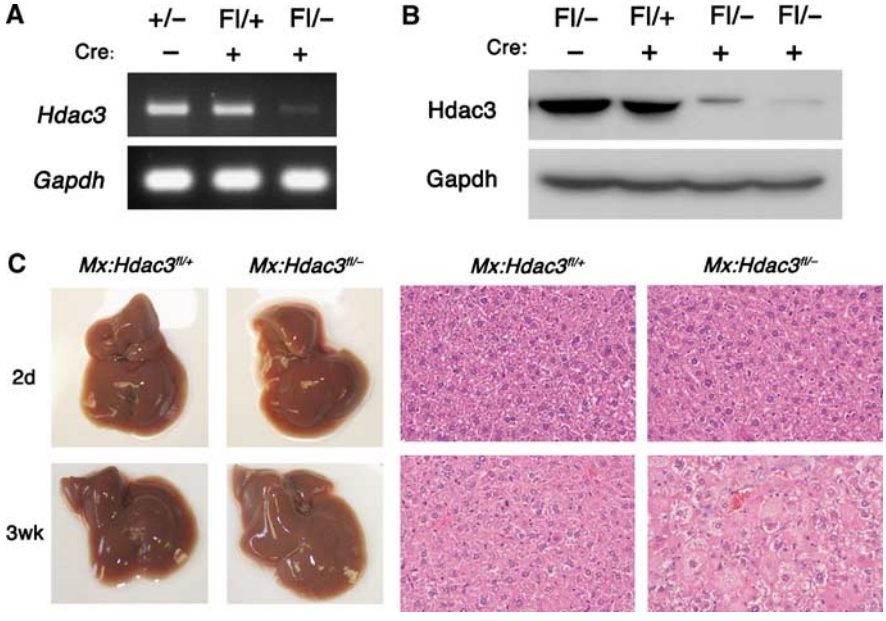

Figure 1 Inducible deletion of *Hdac3* using *Mx1-Cre*. (**A**) RT–PCR was used to detect *Hdac3* mRNA levels in whole-liver extracts and (**B**) western blot analysis detected Hdac3 protein in whole-cell lysates of livers from mice of the indicated genotypes 2 days after the final injection of pIpC. (**C**) Gross morphology (left-hand panels) of control and *Hdac3*-null livers at 2 days and 3 weeks after pIpC injection. The right-hand panels show H&E-stained sections (×400) from the livers shown in the left-hand panels.

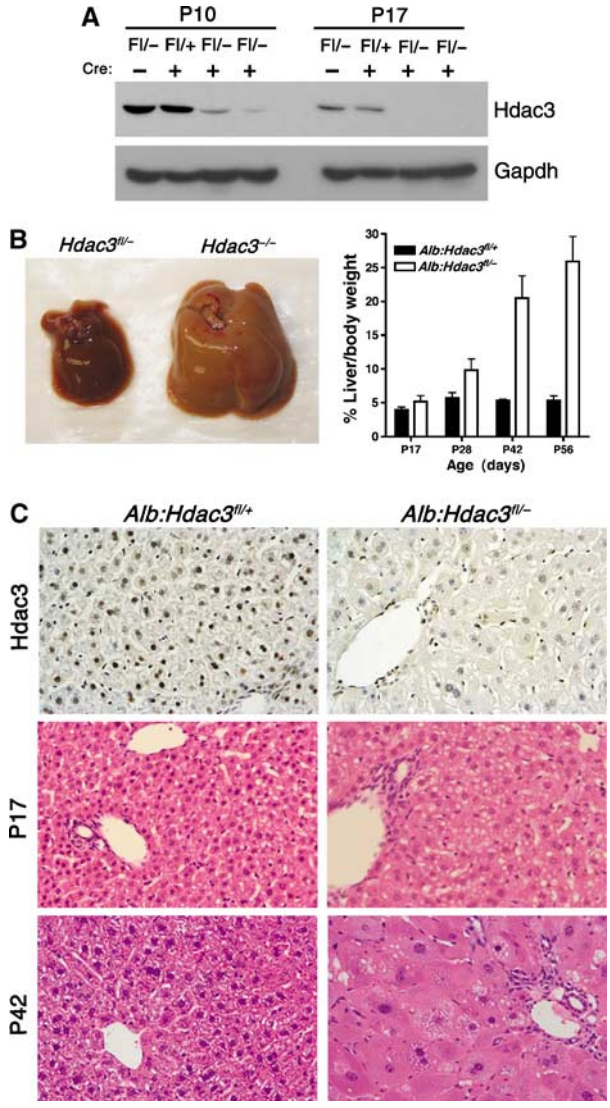

Figure 2 Constitutive deletion of *Hdac3* using liver-specific *Alb-Cre*. (**A**) Hdac3 western blot analysis of liver extracts of 10- or 17-day-old mice of the indicated genotypes. (**B**) Deletion of *Hdac3* results in liver hypertrophy over time. Representative photographs of P42 control and *Hdac3*-null livers are shown. The graph depicts the ratio of liver weight to gross animal weight between 17 and 56 days of age (P17, $P=0.0001$; P28, $P=0.0001$; P42, $P=0.0013$; P56, $P=0.0001$). Statistics were generated using the Student's *t*-test. (**C**) Immunohistochemistry for Hdac3 in P28 liver tissue ($\times 200$) is shown in the upper panels, and histological analysis using H&E-stained sections ($\times 400$) of *Hdac3*-null livers isolated from mice of the indicated ages is shown in the lower panels. Littermate controls are depicted in the left-hand panels.

analysis also indicated that the levels of Hdac1 or Hdac2 were not upregulated to compensate for the loss of *Hdac3* in *Alb:Hdac3*$^{fl/-}$ livers (data not shown).

At P17 the livers appeared normal, but by P28 the livers were pale and hypertrophic, and this trend continued into adulthood. Although the pups were weaned at P21, it is unlikely that the altered morphology was due to the weaning transition, as similar changes were observed in the *Mx1-Cre* model (Figure 1C). The ratio of liver weight to body weight increased from roughly 5% in the heterozygous mice to 25–30% in *Alb:Hdac3*$^{fl/-}$ mice (Figure 2B), and immunohistochemical staining demonstrated complete loss of Hdac3 in hepatocytes (Figure 2C, upper panels). Haematoxylin and eosin (H&E)-stained liver sections indicated that, similar to the *Mx1-Cre* model (Figure 1), *Alb:Hdac3*$^{fl/-}$ livers contained hepatocytes with abnormal cytoplasm starting at P17, and later became hypertrophic (Figure 2C, lower panels).

Deletion of Hdac3 leads to increased hepatocellular damage

The increase in hepatocyte size correlated with the increased organ size, suggesting that altered cell size rather than increased cell number was the basis of the hepatomegaly. To test this model, we examined cell death and proliferation in *Alb:Hdac3*$^{fl/-}$ mice. At P17, there was no significant increase in the number of proliferating cells, as measured by Ki67 immunohistochemistry (Supplementary Figure S2A) or BrdU incorporation (Supplementary Figure S2B). At 6–8 weeks after birth when the number of cycling cells in the livers of control mice had decreased to ~1%, *Hdac3*-null livers retained increased numbers of BrdU-positive hepatocytes (Supplementary Figure S2B). To assess the amount of cellular death and damage occurring at P17, we used TUNEL to detect apoptosis and serum alanine transaminase (ALT) levels to detect hepatotoxicity. The numbers of TUNEL-positive cells were uniformly low and no increase was detected in the P17 (Supplementary Figure S2C) or P28 (data not shown) *Hdac3*-null livers. By contrast, ALT levels were already elevated at P17 and remained high over time (Supplementary Figure S2D), which indicated cellular damage. This may suggest that the increase in cycling cells detected at P28 in *Hdac3*-null livers was a response to cellular damage.

Loss of Hdac3 disrupts metabolic homeostasis

By 4–6 weeks of age, *Alb:Hdac3*$^{fl/-}$ mice were smaller than their littermates and this general growth defect was maintained into adulthood, suggesting a possible defect in metabolism (Figure 3A). By 6–8 weeks of age, *Alb:Hdac3*$^{fl/-}$ mice were visibly leaner, and their visceral adipose tissue was substantially reduced (Figure 3B). Histological analysis of liver sections for glycogen storage using periodic acid Schiff (PAS) demonstrated a dramatic depletion of glycogen in both *Alb:Hdac3*$^{fl/-}$ and *Mx:Hdac3*$^{fl/-}$ hepatocytes compared to heterozygous littermates of the same age (Figure 3C). By contrast, when liver sections from these mice were stained for neutral lipids using Oil Red O, there was a significant increase in the amount of lipid in both *Alb:Hdac3*$^{fl/-}$ and *Mx:Hdac3*$^{fl/-}$ mice compared to control livers (Figure 3D), demonstrating an imbalance between carbohydrate and lipid metabolism.

Metabolism was further examined by quantifying the levels of triglycerides, cholesterol, free fatty acids, HDL, and LDL in both the liver and the serum of *Alb:Hdac3*$^{fl/-}$ mice by mass spectrometry. By P17, the levels of triglycerides in *Alb:Hdac3*$^{fl/-}$ liver samples were dramatically increased (up to 17-fold) compared to controls, and remained continuously high as the mice aged (Table I). Total tissue cholesterol gradually increased in *Hdac3*-null livers, accumulating to levels two-fold higher than in control mice, including unesterified cholesterol (data not shown) and cholesterol esters (Table I). Likewise, there was a very significant increase in serum triglycerides, total serum cholesterol, and LDL in *Alb:Hdac3*$^{fl/-}$ mice as they aged (Table II). Thus, the export of lipids and cholesterol from the liver was not inhibited due to the loss of *Hdac3*, and the synthesis of lipids and

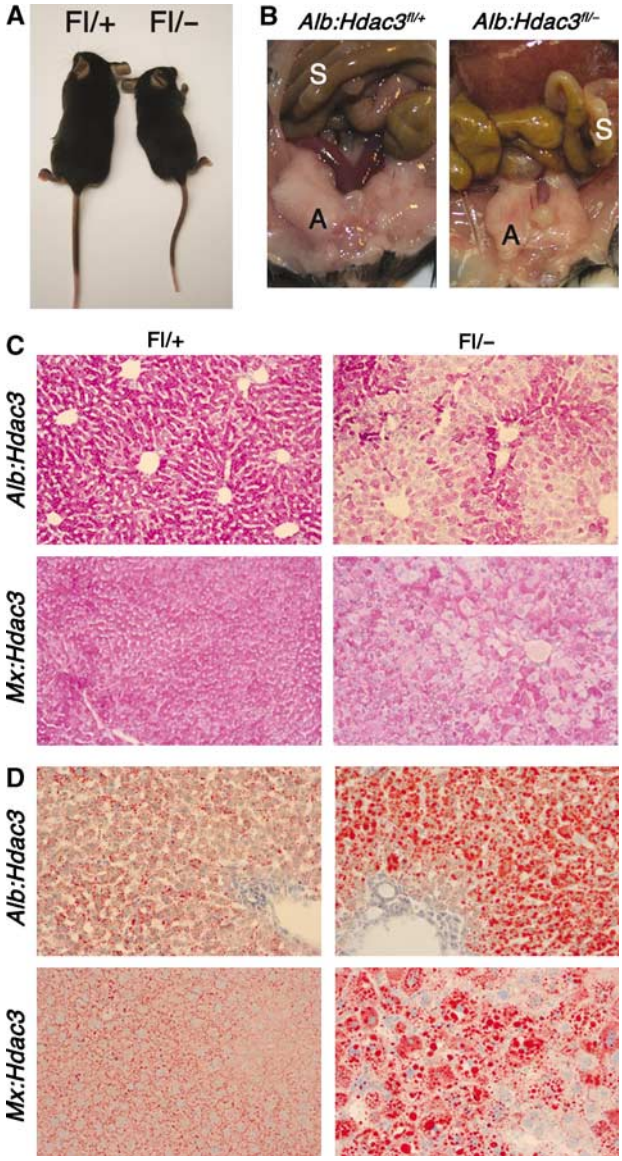

Figure 3 Loss of *Hdac3* significantly alters metabolism. (**A**) *Alb:Hdac3*$^{fl/-}$ mice are smaller than littermate controls, starting at 4 weeks of age. Control animal is depicted to the left in the photo. (**B**) Representation of the decrease in visceral adipose tissue in 15-week-old female *Alb:Hdac3*$^{fl/-}$ mice (right panel). S, small intestine; A, visceral adipose tissue. Note that the liver in the *Alb:Hdac3*$^{fl/-}$ mouse extends into the photo whereas the normal-sized liver in the wild type is not visible in this frame. (**C**) Decrease in glycogen as detected by PAS stain and (**D**) accumulation of lipid droplets as detected by Oil Red O stain of *Alb:Hdac3*$^{fl/-}$ (P17) and *Mx:Hdac3*$^{fl/-}$ (2 weeks after final pIpC injection) livers ($\times 100$). Littermate controls are shown in the left-hand panels.

cholesterol in the liver was increased, leading to their accumulation in the tissue and serum.

Because of the increase in serum triglycerides and LDL starting in mice only 17 days old, we investigated the effects these increases would have on the levels of glucose and its regulatory hormones. In P17 animals, we found similar levels of glucose and insulin in the serum of control and *Alb:Hdac3*$^{fl/-}$ mice, and slightly lower glucagon levels in *Hdac3* liver-specific knockout mice. However, by P28, glucose levels had decreased in *Alb:Hdac3*$^{fl/-}$ mice and, by 6 weeks of age, the mice were hypoglycaemic with only half of the normal serum glucose levels. The hypoglycaemia was accompanied by dramatically lower levels of insulin beginning at P28 that persisted as *Alb:Hdac3*$^{fl/-}$ mice aged. Glucagon levels increased by almost two-fold in the P28 *Alb:Hdac3*$^{fl/-}$ animals, but returned to levels similar to control animals by 6 weeks of age, even though the glucose and insulin levels were still significantly lower than normal levels (Figure 4A).

The hypoglycaemia and the low insulin levels suggested that *Alb:Hdac3*$^{fl/-}$ mice were hypersensitive to insulin. Therefore, we performed a glucose tolerance test on both control and *Alb:Hdac3*$^{fl/-}$ mice. In 10-week-old animals, the fasting glucose levels in *Hdac3* liver-specific null mice were almost two-fold lower than that in littermate control mice (Figure 4B, 0 min time point). Twenty minutes after the injection of glucose, the levels of glucose peaked in a similar fashion in both control and *Alb:Hdac3*$^{fl/-}$ animals, and returned to near-basal levels within 2 h, with a subtly quicker response in *Alb:Hdac3*$^{fl/-}$ mice (Figure 4B). Thus, despite hypoglycaemia and the high levels of triglycerides and cholesterol in *Alb:Hdac3*$^{fl/-}$ mice, these animals responded normally to an insulin-dependent glucose challenge.

Table I Quantification of metabolic parameters in *Alb:Hdac3* liver tissue

Parameter	Age	*Alb:Hdac3*$^{fl/+}$	*Alb:Hdac3*$^{fl/-}$	*P*-value
TG	P17	3.634 ± 0.821	57.674 ± 29.710	0.0036
	P28	3.03 ± 0.996	22.6275 ± 9.343	0.017
	P42	6.03 ± 3.156	20.75 ± 5.836	0.018
	P56	3.3025 ± 1.352	15.05 ± 2.813	0.0003
FFA	P17	1.29 ± 0.057	1.32 ± 0.099	NC
	P28	0.737 ± 0.345	1.3025 ± 0.229	0.046
	P42	0.463 ± 0.153	0.633 ± 0.248	0.37
	P56	0.895 ± 0.295	1.2175 ± 0.392	0.24
T. Chol.	P17	3.34 ± 1.300	1.706 ± 0.472	0.03
	P28	1.203 ± 0.188	1.5825 ± 0.068	0.012
	P42	1.823 ± 0.485	2.786 ± 0.710	0.12
	P56	1.3325 ± 0.106	2.81 ± 0.314	0.0001
CE	P17	1.365 ± 0.403	0.61 ± 0.226	0.0071
	P28	0.453 ± 0.153	0.695 ± 0.223	0.17
	P42	0.476 ± 0.227	1.016 ± 0.235	0.046
	P56	0.3375 ± 0.075	1.5 ± 0.195	0.0001

Averages were calculated (n = at least 4) and include standard deviations for indicated time points. All values are expressed in units of μg/mg. TG, triglycerides; FFA, free fatty acids; T. Chol., total cholesterol; CE, cholesterol esters; NC, no change; *P*-values were calculated using Student's *t*-test.

Lipid and cholesterol biosynthesis regulatory genes are de-repressed after inactivation of Hdac3

A major function of HDACs is the regulation of transcription through deacetylation of histones and non-histone proteins. Therefore, to define the mechanism by which inactivation of *Hdac3* affected liver function, we compared gene expression in the livers of *Alb:Hdac3*$^{+/+}$, *Alb:Hdac3*$^{fl/+}$, and *Alb:Hdac3*$^{fl/-}$ mice. At P17, *Hdac3*-null livers showed only modest alterations in gross organ morphology, and the liver was no longer populated by *Hdac3*-expressing haematopoietic progenitor cells, whereas P28 mice displayed more morphological changes. Thus, we used cDNA microarray analysis at these two time points to address primary and secondary changes in gene expression patterns.

Table II Quantification of metabolic parameters in *Alb:Hdac3* serum

Parameter	Age	*Alb:Hdac3*$^{fl/+}$	*Alb:Hdac3*$^{fl/-}$	*P*-value
TG	P17	58.333 ± 6.501	145.2 ± 42.833	0.0021
	P28	73 ± 15.133	90 ± 38	0.51
	P42	87.333 ± 23.714	234.667 ± 131.5	0.13
	P56	108.75 ± 25.395	403 ± 139.817	0.0061
T. Chol.	P17	144.5 ± 12.582	146.4 ± 32.083	0.9
	P28	93.333 ± 13.051	182.667 ± 24.007	0.0048
	P42	95.667 ± 14.224	236.333 ± 31.005	0.002
	P56	109.25 ± 14.268	327 ± 32.424	0.0001
HDL	P17	55.667 ± 7.638	33.667 ± 11.93	0.055
	P28	36 ± 5.568	53.333 ± 8.145	0.038
	P56	42.25 ± 4.193	60[a]	
LDL	P17	84.333 ± 14.572	100.333 ± 21.825	0.35
	P28	42.667 ± 10.97	111.333 ± 12.858	0.0021
	P56	45.25 ± 10.404	260[a]	

Averages were calculated (n = at least 4) and include standard deviations for indicated time points. All values are expressed in units of mg/dl. TG, triglycerides; T. Chol., total cholesterol; HDL, high-density lipoprotein; LDL, low-density lipoprotein.
[a]TG level over 400 mg/dl invalidates calculations for LDL and HDL, so only select mice could be used in the analysis.

At P17, the major classes of de-regulated genes were involved in metabolism including lipid, fatty acid, steroid, and carbohydrate production, metabolic transport, and cytochromes P450 (Table III). Q-RT–PCR of alternate mRNA samples showed excellent correspondence between the changes observed in the microarray assays and manual validation (Supplementary Figure S4). A large number of these genes are regulated by nuclear hormone receptors, such as PPARs, THR, liver X receptor, and retinoid X receptor. Of significance, a number of key rate-limiting enzymes that control metabolic functions were upregulated. For example, acetyl CoA carboxylase (*Acacb*) regulates the amount of fatty acids in the cell (Widmer *et al*, 1996), and its expression was increased ~21-fold. Squalene epoxidase (*Sqle*, ~173-fold increase) regulates one of the final catalytic reactions of cholesterol biosynthesis (Xu *et al*, 2005; Clapham and Arch, 2007). The final step in the synthesis of cholesterol is catalysed by sterol 14 α-demethylase (Debeljak *et al*, 2003) (also known as *Cyp51*), and the mRNA levels for *Cyp51* were ~22-fold higher in *Hdac3*-null livers (Table III). Thus, *Hdac3* is required for the regulation of genes that control key steps in lipid and cholesterol biosynthesis early in the postnatal liver.

Although the majority of genes that were upregulated at P17 are related to metabolism, a number of transcription factors, including nuclear hormone receptor gene targets, and cell signalling regulatory molecules were also de-regulated (Table III). In addition, genes that contribute to the PI3K/Akt and MAP/ERK pathways, which are linked to cellular stress and cell size regulation, increased from P17 to P28. Genes encoding structural proteins, such as actin and keratin, became increasingly upregulated at p28 (Table III), which correlated with increased cell size, and these changes in gene expression were more likely due to the necessary compensation of the cell to support its abnormal growth than due to transcriptional control by Hdac3. Thus, the microarray data demonstrate that Hdac3 is not only a key regulator of metabolism in the liver, but may also be required for cross-talk between multiple pathways, which leads to complex secondary changes in hepatocellular gene expression over time.

Hdac3 inactivation affects histone acetylation

To further probe the primary molecular mechanism underlying the altered liver function in *Alb:Hdac3*$^{fl/-}$ mice, we examined global histone acetylation *in vivo* by western blot analysis. At 17 days after birth when there is complete depletion of *Hdac3* and dramatic changes in gene expression profiles, we found modest increases in the acetylation of histone H4K5, H4K8, and H4K12, but variable changes in H3K9 (Figure 5A). Similar results were found using chromatin immunoprecipitation (ChIP) of promoter regions of genes upregulated in the microarray analysis (Figure 5B). Although some N-terminal histone residues have been identified as preferential substrates for Hdac3 (Hartman *et al*, 2005), the promoter regions of de-repressed genes, such as *Sqle* and *Acacb*, had a general increase in acetylated histone residues. There was also increased acetylation in the coding region of *Cyp51* (exon 5) and at the promoter of *N-CoR*, which was not transcriptionally activated in the absence of *Hdac3* (Figure 5B). General increases in acetylation at both the global level and at specific genomic regions suggest that altered histone acetylation contributes to the changes in gene expression in *Hdac3*-null livers, although hyperacetylation of other proteins may also be a contributing factor.

Loss of Hdac3 increases Pparγ expression and activity in hepatocytes

Gene expression analysis identified multiple transcriptional networks that were disrupted at both the P17 and P28 time points and are regulated by nuclear hormone receptors that recruit Hdac3. At P17, one of these networks was centered around Pparγ, which is not the predominant Ppar family member normally expressed in the liver (Zhu *et al*, 1993). By P28, an even greater number of Pparγ targets were upregulated, as part of a larger network regulated by nuclear hormone receptors (Supplementary Figure 3). Pparγ is a key regulator of metabolic homeostasis, specifically in adipocytes, and this hormone receptor recruits the Hdac3/N-CoR repression complex (Fajas *et al*, 2002; Guan *et al*, 2005). Although not normally highly expressed in the liver, the transcript level of *Pparγ*, but not *Pparα* or *Pparβ*, was

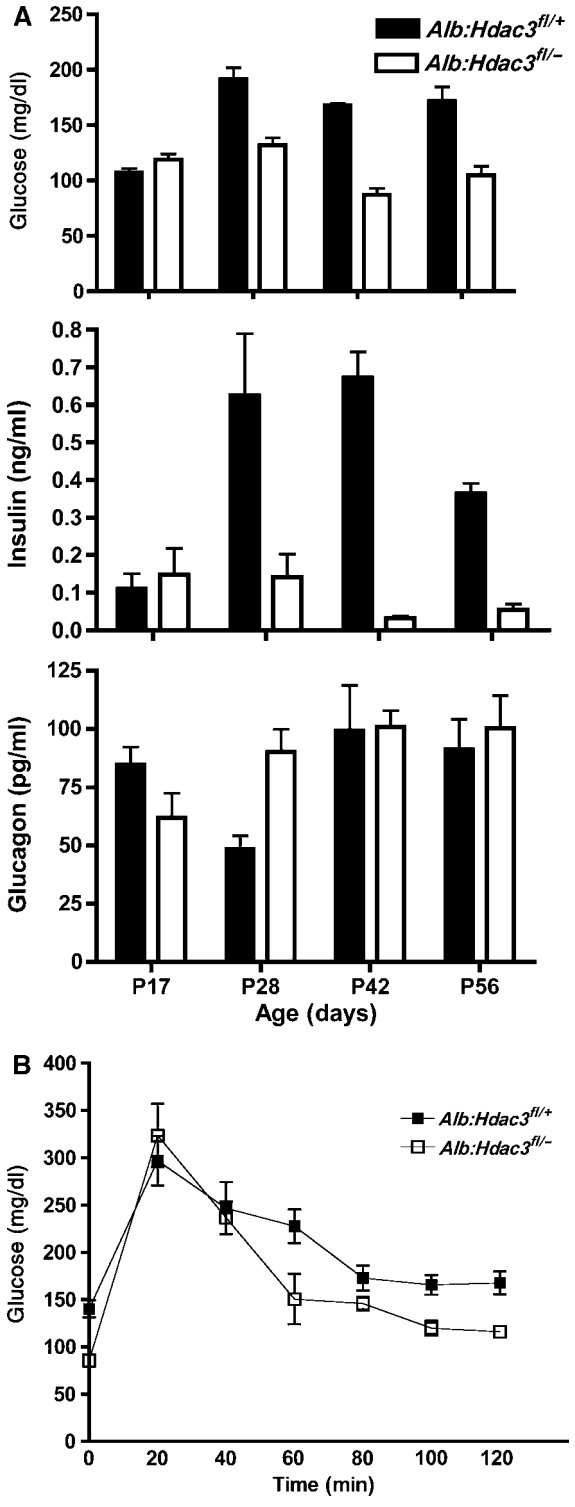

Figure 4 *Alb:Hdac3*$^{fl/-}$ mice are hypoglycaemic and are insulin sensitive. (**A**) Graphical representation of whole-blood measurements of glucose (P17, $P=0.065$; P28, $P=0.0001$; P42, $P=0.0002$; P56, $P=0.0006$) and the serum levels of insulin (P17, $P=0.63$; P28, $P=0.02$; P42, $P=0.0001$; P56, $P=0.0001$) and glucagon (P17, $P=0.062$; P28, $P=0.021$; P42, $P=0.9$; P56, $P=0.66$) at the indicated time points in *Alb:Hdac3* mice. (**B**) The glucose tolerance test was performed in 10-week-old *Alb:Hdac3* mice, which were fasted for 6 h before a dose of 1.5 mg/g glucose. Glucose levels were measured at the indicated time points over a 2-h period. (0′, $P=0.0012$; 20′, $P=0.54$; 40′, $P=0.78$; 60′, $P=0.054$; 80′, $P=0.14$; 100′, $P=0.013$; 120′, $P=0.0082$). Statistics were generated using the Student's *t*-test.

increased by ~3-fold, and Pparγ protein levels were also increased in *Alb:Hdac3*$^{fl/-}$ mice (Figure 6A). In addition, *Pparγ* was upregulated four-fold in *Mx:Hdac3*$^{fl/-}$ mice up to 2 weeks after the last injection of pIpC (data not shown). Pparγ exists in two isoforms (Pparγ1 and Pparγ2), which differ in their N-termini (Zhu *et al*, 1993) and have differential functions and activities (Werman *et al*, 1997; Ren *et al*, 2002). Using oligonucleotide primers specific to *Pparγ1* and *Pparγ2* for Q-RT–PCR, we found that *Pparγ2* expression was specifically induced as early as P10 in *Alb:Hdac3*$^{fl/-}$ livers (Figure 6B), which coincided with increased levels of Pparγ-regulated genes, such as *Cd36* (Table III).

To determine the level of contribution of Pparγ to the *Hdac3*-null liver phenotype, the Pparγ inhibitor GW9662 was injected into a cohort of mice daily for 4 weeks. Pparγ inhibition correlated with reduced expression of *Cd36* and *Pdk4* (Figure 6C). Hepatocyte structure was not affected by inhibition of Pparγ, but Oil Red O staining detected a decrease in lipid accumulation in *Alb:Hdac3*$^{fl/-}$ mice treated with GW9662 (Figure 6D, lower right-hand panels). Thus, inhibition of Pparγ partially reversed lipid accumulation in *Hdac3*-null livers, indicating that Pparγ contributes to the increase in lipids upon inactivation of *Hdac3*.

Inhibition of mTOR affects lipid levels in Alb:Hdac3$^{fl/-}$ *mice*

Activation of the PI3K/Akt pathway is involved in cellular homeostasis and metabolic control (Fingar and Blenis, 2004; Hay and Sonenberg, 2004), and increased levels of palmitate activated mTOR, a downstream target of Akt signalling, in primary hepatocytes (Mordier and Iynedjian, 2007). Mass spectrometry analysis uncovered a marked increase in palmitate levels in *Hdac3*-null liver tissue at P17, which remained high through P56 (Figure 7A). This increase was accompanied by increased phosphorylation of ribosomal S6 kinase (S6K), an mTOR substrate (Figure 7B). Therefore, we injected 3-week-old mice with rapamycin, a well-characterized inhibitor of mTOR, daily for 3 weeks. This regimen inhibited mTOR function *in vivo*, as evidenced by the lack of S6K phosphorylation in *Alb:Hdac3*$^{fl/-}$ mice (Figure 7C). The expression levels of transcripts that are regulated by mTOR signalling, such as *Acacb* (Brown *et al*, 2007) and *Glut4* (Hernandez *et al*, 2001), were also downregulated by 2.5- and 8-fold, respectively (Figure 7D). Inhibition of mTOR stunted the growth of both control and *Hdac3*-null mice, but it did not dramatically affect the liver hypertrophy, as rapamycin-treated *Alb:Hdac3*$^{fl/-}$ mice had comparable liver weight/body weight ratios as vehicle-treated *Alb:Hdac3*$^{fl/-}$ mice (Figure 7E). However, treatment with rapamycin decreased the accumulation of neutral lipid in *Alb:Hdac3*$^{fl/-}$ mice (Figure 7F). Thus, in addition to inactivation of nuclear hormone receptor-mediated transcriptional repression, mTOR activation contributes to the phenotypes observed in *Hdac3*-null livers.

Discussion

The genetic analysis of *Hdac3* in postnatal mice, using two separate mouse models of Cre recombinase, indicates that it is an important regulatory component of molecular complexes that control gene expression, which in turn controls metabolic functions in the liver. Loss of *Hdac3* disrupted liver

Table III Transcription changes in *Alb:Hdac3*$^{fl/-}$ mice at P17 and P28

Biological process	Gene name (gene symbol)	Average fold change	
		P17	P28
Metabolism	Acetyl-Coenzyme A Carboxylase beta (Acacb)	21.5850	2.8755
Lipid/fatty acid	Enoyl-Coenzyme A hydratase/3-hydroxyacyl Co-A dehydrogenase (Ehhadh)	3.6582	12.4253
	Stearoyl-Coenzyme A desaturase 1 (Scd1)	3.2483	9.1621
	Acyl-Coenzyme A oxidase 1, palmitoyl (Acox1)	3.8679	2.6733
	Adipose differentiation related protein (Adfp)	3.9698	9.2127
	Apolipoprotein A-IV (Apoa4)	11.6171	32.6144
	Sterol-C4-methyl oxidase-like (Sc4mol)	24.2809	−2.130
	CD36 antigen (Cd36)	1.8733	5.6965
	ELOVL family member 6, elongation of long chain fatty acids	9.6841	5.6540
	Fatty acid desaturase 2 (Fads2)	2.6065	3.3344
	Fatty acid synthase (Fasn)	5.4032	4.3510
	Phospholipase A2, group VI (Pla2g6)	4.1585	3.6305
	Acetoacetyl-CoA synthetase (Aacs)	5.9526	1.0360
	Low density lipoprotein receptor (Ldlr)	2.4232	−1.2550
	Very low density lipoprotein receptor (Vldlr)	6.4971	5.2987
	StAR-related lipid transfer (START) domain containing 4 (Stard4)	3.2569	1.1132
	Cytochrome P450, family 4, subfamily a, polypeptide 12 (Cyp4a12)	27.7789	6.9124
	Cytochrome P450, family 4, subfamily a, polypeptide 14 (Cyp4a14)	3.0869	2.7802
	Cytochrome P450, family 7, subfamily a, polypeptide 1 (Cyp7a1)	2.5207	3.9425
Cholesterol	3-Hydroxy-3-methylglutaryl-Coenzyme A synthase (Hmgcs)	7.9894	1.2339
	Isopentenyl-diphosphate delta isomerase (Idi1)	18.2946	−2.2900
	Farnesyl diphosphate farnesyl transferase 1 (Fdft1)	5.4985	−1.0576
	Farnesyl diphosphate synthetase (Fdps)	13.7628	1.7472
	Squalene epoxidase (Sqle)	172.9337	−1.5849
	Cytochrome P450, 51 (Cyp51)	21.9741	−1.8527
Other	Aldolase 1 (Aldo1)		2.7904
	Glucokinase (Gck)	2.6046	2.7178
	Hexokinase 2 (Hk2)		7.1749
	Insulin induced gene 1 (Insig1)	4.7532	−1.4560
	Insulin-like 6 (Insl6)	2.5668	3.3368
	Aldehyde oxidase 1 (Aox1)	3.1535	1.4061
	Xanthine dehydrogenase (Xdh)	2.1399	1.0452
	Aldehyde dehydrogenase family 3, subfamily A2 (Aldh3a2)	2.5317	3.3068
	Glyceraldehyde 3-phosphate dehydrogenase (Gapdh) (345274)	2.1606	2.6829
Nuclear receptor-related	Serum/glucocorticoid regulated kinase 2 (Sgk2)	3.8111	2.6817
	Thyroid hormone responsive SPOT14 homolog (Thrsp)	33.7453	2.4455
	Retinoic acid early transcript gamma (Raet1b)	6.4309	3.6549
	Retinoic acid early transcript delta (Raet1d)	6.4457	3.4374
	Glucocorticoid modulatory element binding protein 1 (Gmeb1)		2.1215
	Glucocorticoid induced gene 1 (Gig1)		2.7644
	Dopa decarboxylase (Ddc)	3.2737	3.1596
	Peroxisome proliferator activated receptor gamma (Pparγ)		4.7764
Cellular regulation	Dual-specificity tyrosine-(Y)-phosphorylation regulated kinase 3 (Dyrk3)	3.2766	7.4758
	Inositol 1,3,4-triphosphate 5/6 kinase (Itpk1)	2.8298	5.1727
	Dual specificity phosphatase 8 (Dusp8)	2.1698	3.9070
	Protein kinase C, alpha (Prkca)		3.3297
	Ras homolog gene family, member B (Rhob)		3.4098
	Insulin-like growth factor 2 (Igf2)		6.9211
	Mitogen activated protein kinase 3 (Mapk3)		2.3059
Cell cycle	Cyclin A2 (Ccna2)		2.6210
	Cyclin-dependent kinase 6 (Cdk6)	3.2699	2.4362
	Cyclin-dependent kinase inhibitor 1A/P21 (Cdkn1a)		12.1251
	Cyclin-dependent kinase inhibitor 2A/P16 (Cdkn2a)		3.8940
	Myelocytomatosis oncogene (Myc)		4.0527
	Rous sarcoma oncogene (Src)		4.7890
	Jun oncogene (Jun)		3.2893
	Jun proto-oncogene related gene d1(Jund1)	2.7052	3.0491
	Polo-like kinase 2 (Plk2)		2.5635
	Polo-like kinase 3 (Plk3)	3.1039	5.1568
	Polo-like kinase 4 (Plk4)		2.5163
	Topoisomerase (DNA) II alpha (Top2a)		7.1831
Cytoskeletal/structural	Keratin complex 1, acidic, gene 18 (Krt1-18)	4.3301	10.0402
	Keratin complex 2, basic, gene 8 (Krt2-8)	4.3515	9.1991
	Procollagen, type I, alpha 1 (Col1a1)	4.9802	16.6567
	Periplakin (Ppl)	3.0304	3.0085
	Tubulin, alpha 8 (Tuba8)	3.3211	3.4593
	Tubulin, beta 2 (Tubb2)	1.9632	32.2436
	Actin, gamma, cytoplasmic (Actg)		2.5746

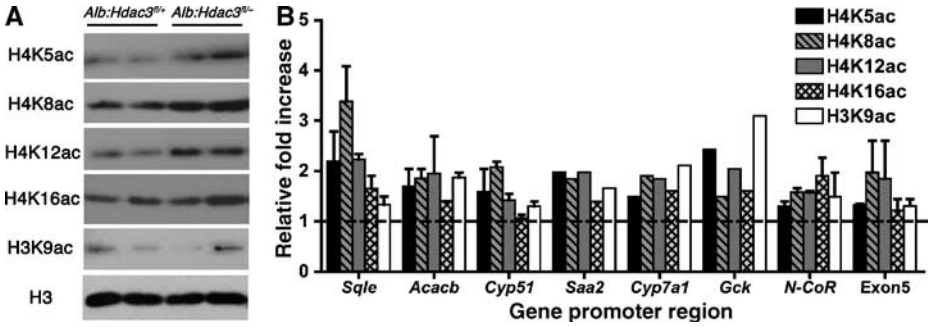

Figure 5 Histone acetylation increases in *Alb:Hdac3*$^{fl/-}$ mice. (**A**) Analysis of histone modifications in P17 liver nuclear lysates with the specified genotypes using the indicated antibodies. (**B**) ChIP of promoters in livers of genes identified as upregulated through microarray analysis and non-transcriptionally activated sequences using antibodies to the indicated acetylated histone residues. Exon5 refers to sequences in exon 5 of *Cyp51*. Data are shown relative to the levels of histone H3, and the increase in *Alb:Hdac3*$^{fl/-}$ mice over controls is denoted by the dashed line.

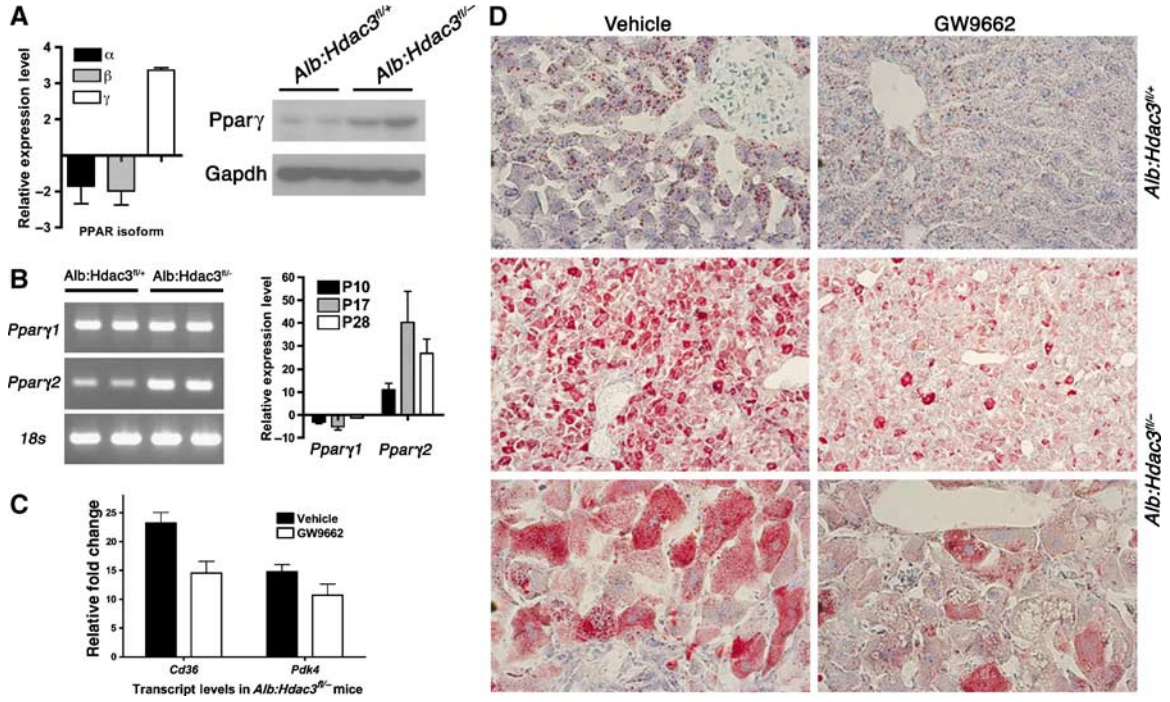

Figure 6 Pparγ is upregulated in the absence of *Hdac3*. (**A**) Detection of Ppar isoforms (*Pparα*, *Pparβ*, and *Pparγ*) in P17 *Hdac3*-null livers by Q-RT–PCR, and western blot analysis of Pparγ in liver whole-cell lysates at P28. Heterozygous littermates were used as controls. (**B**) Differential regulation of the two different isoforms of *Pparγ* in 17-day *Alb:Hdac3* mice is shown in the left-hand panel. Q-RT–PCR of *Pparγ1* and *Pparγ2* levels in *Alb:Hdac3*$^{fl/-}$ mice at the indicated time points is shown in the right-hand panel. (**C**) Q-RT–PCR of the Pparγ target genes, *Cd36* and *Pdk4*, in *Alb:Hdac3*$^{fl/-}$ vehicle- and GW9662-treated mice ($P = 0.029$ and $P = 0.208$, respectively, Student's *t*-test). (**D**) Cohorts of *Alb:Hdac3* mice were treated with vehicle or GW9662, an inhibitor of Pparγ, for 4 weeks and liver tissue was stained with Oil-Red O to detect lipid. The upper panels depict control mice ($\times 400$ magnification) and middle ($\times 100$ magnification) and lower panels ($\times 400$ magnification) depict *Alb:Hdac3*$^{fl/-}$ mice.

cholesterol and lipid homeostasis by de-repressing genes that regulate lipid and steroid metabolism, allowing the accumulation of lipids at the expense of glycogen storage. Although HDACs have many non-histone protein targets for deacetylation (Juan *et al*, 2000; Luo *et al*, 2000; Ashburner *et al*, 2001; Hubbert *et al*, 2002; Shimazu *et al*, 2006; Gregoire *et al*, 2007), the disruption of liver metabolism was evident at the level of transcription and was accompanied by increases in histone acetylation. The regulation of many of these genes can be directly traced to nuclear hormone receptors such as the THR and Pparγ that recruit Hdac3.

Pparγ is the hub of a large gene network that is de-repressed upon deletion of *Hdac3*. The *Pparγ2* isoform was specifically upregulated in *Hdac3*-null livers, potentially through nuclear hormone receptor-mediated regulation (Tontonoz *et al*, 1994; Picard *et al*, 2004). Enforced expression of *Pparγ2* in fibroblasts induced lipogenic gene transcription and activated a differentiation response towards adipocytes (Tontonoz *et al*, 1994). In addition, liver-specific induction of *Pparγ2* in a mouse model of obesity triggered a lipogenic gene programme and hepatic steatosis that is reminiscent of inactivation of *Hdac3* (Yu *et al*, 2003; Zhang *et al*, 2006). Moreover, *Alb:Hdac3*$^{fl/-}$ mice had low levels of

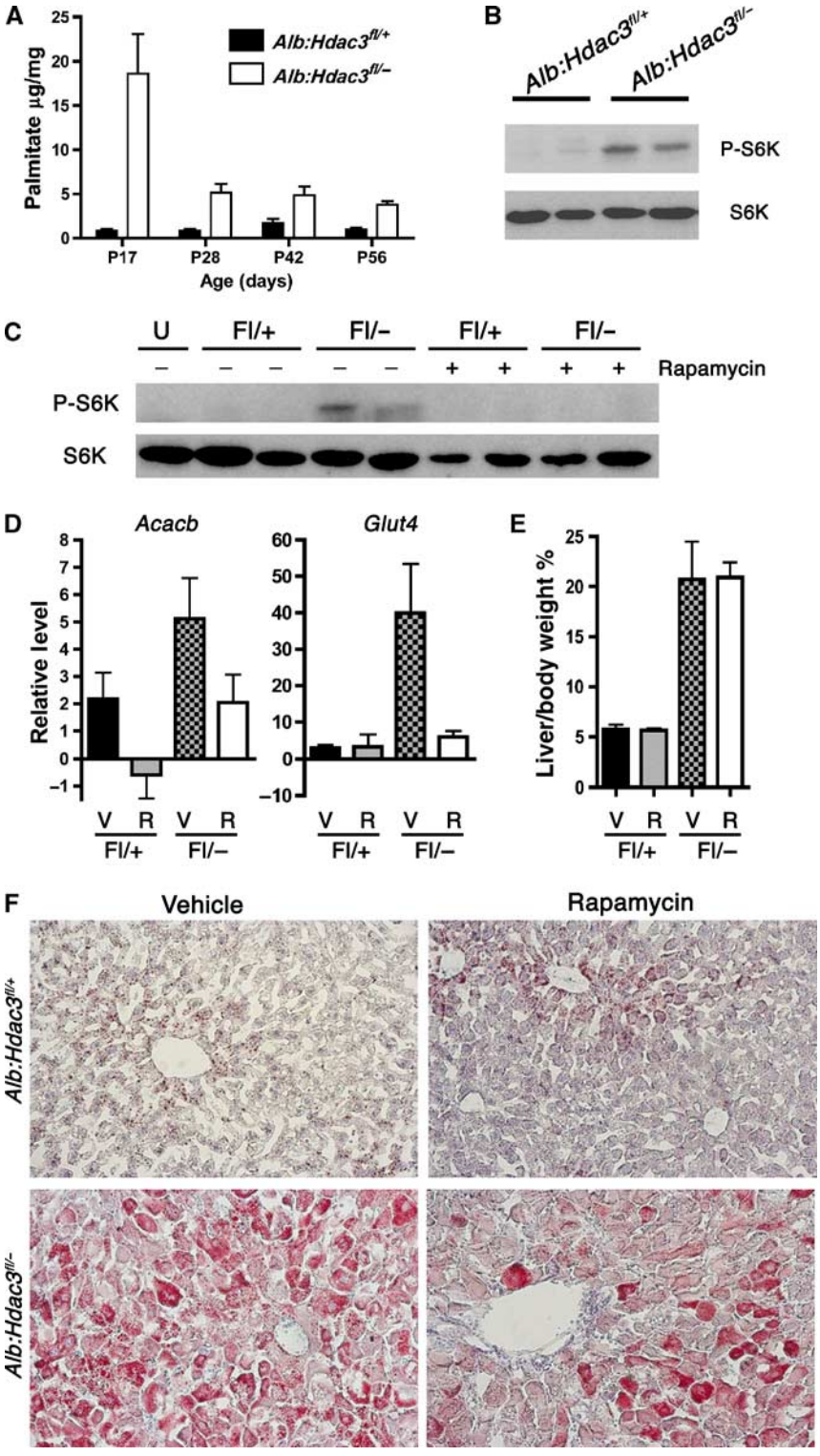

Figure 7 Loss of *Hdac3* activates mTOR, which contributes to disrupted metabolism. (**A**) Palmitate levels in *Hdac3:Alb* mice at P17–P56. (**B**) Western blot analysis of P28 liver whole-cell lysates indicating levels of S6K and phosphorylated S6K (P-S6K). (**C**) Cohorts of *Alb:Hdac3*$^{fl/+}$ and *Alb:Hdac3*$^{fl/-}$ mice were treated with vehicle or rapamycin for 3 weeks, and a representative western blot analysis of S6K and P-S6K indicates inhibition of mTOR after rapamycin treatment. (**D**) Q-RT–PCR of known mRNAs regulated by mTOR in the indicated groups of mice (*Acacb*, $P=0.151$, and *Glut4*, $P=0.015$, using Student's *t*-test). V, vehicle treated; R, rapamycin treated. (**E**) Graphical representation of liver weight/body weight ratio of vehicle-treated, or rapamycin-treated *Alb:Hdac3* mice. V, vehicle treated; R, rapamycin treated. (**F**) Oil-Red O staining of liver tissue from the indicated genotypes, treated with vehicle or rapamycin. The upper panels depict control livers, whereas the lower panels depict *Hdac3*-null livers ($\times 200$ magnification).

insulin and were hypoglycaemic, which is similar to the effects of administration of Pparγ agonists (Lehmann *et al*, 1995). Inhibition of Pparγ with GW9662 decreased lipid accumulation by 20–50% in *Hdac3*-null livers, but it did not consistently affect blood glucose levels (data not shown). Thus, although aspects of the *Hdac3*-null liver phenotype are consistent with phenotypes induced by activation of Pparγ, loss of *Hdac3* disrupts additional metabolic cues that may be regulated by other nuclear hormone receptors or other signalling pathways (Table III).

Alb:Hdac3$^{fl/-}$ livers also contained increased levels of palmitate, which can lead to oxidative stress and trigger lipid-responsive signalling pathways (Mordier and Iynedjian, 2007). Indeed, these pathways were activated as demonstrated by the expression of cellular stress-responsive genes (Table III) and the phosphorylation of S6K (Figure 7). Although constitutively active Akt induced hepatomegaly in mice (Ono *et al*, 2003; Haga *et al*, 2005), rapamycin did not affect cell size in *Hdac3*-null livers (Figure 7). Thus, lipid metabolism, but not hepatocyte hypertrophy, was at least partially dependent on the mTOR/raptor complex, which is sensitive to rapamycin (Loewith *et al*, 2002; Jacinto *et al*, 2004).

The primary targets of HDIs in clinical trials are class I HDACs (Marks *et al*, 2001). *Alb:Hdac3*$^{fl/-}$ phenotypes have major implications for drugs targeting these enzymes. Liver function was dramatically disrupted when *Hdac3* was constitutively removed (*Alb-Cre* mice), yet the mice survived and were leaner, albeit with high levels of cholesterol, high triglycerides, and low blood sugar. This indicates that HDIs may transiently affect liver metabolism. Most of these compounds have relatively short half-lives *in vivo*, which may be a major benefit, as liver function would only be partially impaired. In addition, the *Mx1-Cre* model indicated that any toxic side effects of disruption of Hdac3 function are likely reversible. That is, it appeared that 4–5 weeks after Cre induction, *Hdac3* expression and liver morphology normalized (SK Knutson, unpublished data). Thus, even if complete inactivation of Hdac3 could be achieved by continual infusion of an HDI, by terminating therapy the liver would be expected to recover, and pulse therapy would be expected to be relatively safe. Nevertheless, in dire cases where HDI therapy may have a major impact on the survival of the patient, even continuous infusion may be tolerated for several weeks. However, the changes in *Alb:Hdac3*$^{fl/-}$ livers are similar to the initiating events in non-alcoholic fatty liver disease, which include increases in lipid accumulation and cellular hypertrophy (reviewed by Sanyal, 2005). Therefore, long-term treatment with this regimen may ultimately have severe side effects, similar to those observed in *Alb:Hdac3*$^{fl/-}$ mice.

Materials and methods

Description of mice

Mice harbouring a conditional allele (fl) or a null allele (−) of *Hdac3* were crossed to transgenic mice expressing *Mx1-Cre* (Kuhn *et al*, 1995) or *Alb-Cre* (Postic *et al*, 1999; Postic and Magnuson, 2000). The offspring from these mice were then bred to yield mice with a conditional allele in conjunction with either a wild-type (fl/+) or null allele (fl/−), and *Cre*. To induce Cre expression in *Mx1-Cre*-expressing mice, 5-week-old animals received an intraperitoneal (i.p.) injection of 500 μg pIpC in PBS every other day for 13 days, for a total of seven injections, with the last day of injection being denoted as day 0. Mice were killed at 1 day, 2 days, and 1, 2, 3, 4, and 5 weeks after the last injection.

Three-week-old *Alb:Hdac3* mice were used in both GW9662 (Cayman Chemicals) and rapamycin (LC Laboratories) studies. For GW9662 experiments, mice were injected with 2 mg/kg, daily for 4 weeks. For rapamycin experiments, mice were injected with 10 mg/kg, daily for 3 weeks.

Preparation of liver lysates and western blot analysis

Whole-cell lysates were made by homogenizing in PBS plus 0.5% Triton X-100, 0.1% DOC, and 0.1% SDS, sonicated and cleared by centrifugation. Lysates were subjected to 10 or 12% SDS–PAGE, transferred to a PVDF membrane (Millipore), blocked with 5% non-fat dry milk for 1 h, incubated with primary antibody at 4°C and secondary antibody for 1–3 h at room temperature, and developed using SuperSignal West Pico reagents (Pierce).

Antibodies

The following antibodies were obtained from Upstate Cell Signaling: histone H3 (05-928), histone H4 (07-108), acetyl-histone H4 (Lys5) (07-327), acetyl-histone H4 (Lys8) (06-760), acetyl-histone H4 (Lys12) (06-761), acetyl-histone H4 (Lys16) (07-329), and acetyl-histone H3 (Lys9) (06-942). The antibodies for Hdac3 (ab-32369-100 and ab3279), histone H4K5ac (ab51997), histone H4K12ac (ab1761), and GAPDH (clone 6C5, ab8245) were obtained from Abcam. The antibody for Pparγ (sc-7196) was obtained from Santa Cruz. The p70 S6 Kinase (#2708) and phospho-p70 S6 Kinase (Thr398; #9206) antibodies were obtained from Cell Signaling Technology.

Histology and immunohistochemistry

The tissue was fixed in 4% paraformaldehyde at 4°C, dehydrated, and embedded in paraffin. Sections (5 μm) were stained with H&E and PAS. Apoptotic cells were detected by TUNEL using the ApopTag Plus Kit (Chemicon International). Cycling cells were detected by injecting the mice i.p. with 100 μg/g BrdU in PBS 1 h before they were killed. BrdU was detected using anti-BrdU for immunohistochemistry and BrdU-positive cells were counted per 100 nuclei in control and *Hdac3*-null liver sections. Frozen sections were prepared by fixing the tissue in 4% paraformaldehyde at 4°C for 2 h followed by 30% sucrose for 3–12 h. The tissue was then embedded in OCT, frozen on dry ice, and 10 μm sections were stained with Oil Red O and counterstained with haematoxylin.

DNA and RNA extraction, Q-RT–PCR, and microarray analysis

Genomic tail DNA was used for preliminary genotyping. Liver DNA was purified using the Qiagen DNeasy Tissue Kit. Liver RNA was extracted using the Versagene RNA Tissue Kit (Gentra Systems). cDNA was prepared from 2 to 3 μg RNA using random hexanucleotide primers (Applied Biosystems) and M-MLV Reverse Transcriptase (Promega). For Q-RT–PCR, cDNA was analysed using iQ SYBR Green Supermix (Bio-Rad). Primer sequences are available on request.

For the microarray analysis, RNA was prepared from individual whole livers, tested for RNA quality, and high-quality RNA from 10 control and 10 *Hdac3*-null livers was pooled to normalize for biological variability between animals before being hybridized to Applied Biosystems 1700 Mouse Expression Array System chips for analysis in the Vanderbilt Microarray Shared Resource. Biological replicates of pools were performed to further normalize for biological variability and a total of at least three arrays were performed for each genotype and each time point. The data were analysed using GeneSpring (Agilent Technologies) and genes whose expression changed at least two-fold using a *t*-test were included in the data sets. Ingenuity Pathway Analysis software (Ingenuity Systems, Mountain View, CA) and Panther Classification System software were used to group the regulated genes into ontology groups (Thomas *et al*, 2003; Mi *et al*, 2007).

Chromatin immunoprecipitation

The ChIP assay was performed following the standard protocol of the Chromatin Immunoprecipitation Assay Kit from Upstate Cell Signaling, with slight modifications using minced tissue for formaldehyde crosslinking. DNA was purified using the Qiagen PCR Purification Kit. Primers designed to the designated promoter sequences were used for quantification of histone acetylation using

Q-PCR, with histone H3 and input sonicated DNA as reference controls.

Metabolic analysis

Serum levels of ALT were measured using the ALT Reagent Colorimetric Endpoint Method (Teco Diagnostics) following the standard protocol with slight modifications. Glucose levels were measured in whole blood using the Free Style Flash glucose monitor (courtesy of Dr William Russell). Serum levels of insulin and glucagon were measured using a double-antibody radioimmunoassay, with all primary reagents supplied by Linco Research Inc. (St Charles, MO). Hormone levels were determined by the Vanderbilt Diabetes Center Hormone Assay Core. To perform the glucose tolerance test, 10-week-old mice were fasted for 6 h and injected i.p. with glucose at 1.5 mg/g body weight. Blood glucose levels were measured through the tail tip using the Free Style Flash glucose monitor during the indicated time course. Total plasma cholesterol and triglycerides were measured by standard enzymatic assays. Liver tissue extraction and analysis of lipids and cholesterol were performed by the Vanderbilt Mouse Metabolic Phenotyping Center (MMPC) Analytical Resources Core, as previously described (Zhu *et al*, 2005).

Supplementary data

Supplementary data are available at *The EMBO Journal* Online (http://www.embojournal.org).

Acknowledgements

We thank the members of the Hiebert lab for helpful discussions and encouragement, and the Vanderbilt-Ingram Cancer Center (CA68485) and the Vanderbilt Digestive Diseases Research Center (5P30DK58404) for support and the use of shared resources including flow cytometry, microarray analysis, DNA sequencing, transgenic/embryonic stem cell, immunohistochemistry, and histological analysis. This work was supported by the TJ Martell Foundation, the National Institutes of Health (NIH) grants RO1-CA64140 and RO1-CA77274 (SWH), and Leukemia and Lymphoma Society postdoctoral fellowship #5074-03 (BJC) and by T32 CA009385 (SKK).

References

Alcalay M, Zangrilli D, Pandolfi PP, Longo L, Mencarelli A, Giacomucci A, Rocchi M, Biondi A, Rambaldi A, Lo Coco F, E, F, PG (1991) Translocation breakpoint of acute promyelocytic leukemia lies within the retinoic acid receptor alpha locus. *Proc Natl Acad Sci USA* **88:** 1977–1981

Amann JM, Nip J, Strom DK, Lutterbach B, Harada H, Lenny N, Downing JR, Meyers S, Hiebert SW (2001) ETO, a target of t(8;21) in acute leukemia, makes distinct contacts with multiple histone deacetylases and binds mSin3A through its oligomerization domain. *Mol Cell Biol* **21:** 6470–6483

Ashburner BP, Westerheide SD, Baldwin Jr AS (2001) The p65 (RelA) subunit of NF-kappaB interacts with the histone deacetylase (HDAC) corepressors HDAC1 and HDAC2 to negatively regulate gene expression. *Mol Cell Biol* **21:** 7065–7077

Bhaskara S, Chyla BJ, Amann JM, Knutson SK, Hiebert SW (2008) Deletion of *Histone Deacetylase 3* reveals critical roles in S-phase progression and DNA damage control. *Molecular Cell* (in press)

Brown NF, Stefanovic-Racic M, Sipula IJ, Perdomo G (2007) The mammalian target of rapamycin regulates lipid metabolism in primary cultures of rat hepatocytes. *Metabolism* **56:** 1500–1507

Chakrabarti SR, Nucifora G (1999) The leukemia-associated gene TEL encodes a transcription repressor which associates with SMRT and mSin3A. *Biochem Biophys Res Commun* **264:** 871–877

Clapham JC, Arch JR (2007) Thermogenic and metabolic antiobesity drugs: rationale and opportunities. *Diabetes Obes Metab* **9:** 259–275

de Ruijter AJ, van Gennip AH, Caron HN, Kemp S, van Kuilenburg AB (2003) Histone deacetylases (HDACs): characterization of the classical HDAC family. *Biochem J* **370:** 737–749

Debeljak N, Fink M, Rozman D (2003) Many facets of mammalian lanosterol 14alpha-demethylase from the evolutionarily conserved cytochrome P450 family CYP51. *Arch Biochem Biophys* **409:** 159–171

Fajas L, Egler V, Reiter R, Hansen J, Kristiansen K, Debril MB, Miard S, Auwerx J (2002) The retinoblastoma-histone deacetylase 3 complex inhibits PPARgamma and adipocyte differentiation. *Dev Cell* **3:** 903–910

Fenrick R, Amann JM, Lutterbach B, Wang L, Westendorf JJ, Downing JR, Hiebert SW (1999) Both TEL and AML-1 contribute repression domains to the t(12;21) fusion protein. *Mol Cell Biol* **19:** 6566–6574

Fenrick R, Wang L, Nip J, Amann JM, Rooney RJ, Walker-Daniels J, Crawford HC, Hulboy DL, Kinch MS, Matrisian LM, Hiebert SW (2000) TEL, a putative tumor suppressor, modulates cell growth and cell morphology of ras-transformed cells while repressing the transcription of stromelysin-1. *Mol Cell Biol* **20:** 5828–5839

Fingar DC, Blenis J (2004) Target of rapamycin (TOR): an integrator of nutrient and growth factor signals and coordinator of cell growth and cell cycle progression. *Oncogene* **23:** 3151–3171

Fischle W, Dequiedt F, Hendzel MJ, Guenther MG, Lazar MA, Voelter W, Verdin E (2002) Enzymatic activity associated with class II HDACs is dependent on a multiprotein complex containing HDAC3 and SMRT/N-CoR. *Mol Cell* **9:** 45–57

Gallinari P, Di Marco S, Jones P, Pallaoro M, Steinkuhler C (2007) HDACs, histone deacetylation and gene transcription: from molecular biology to cancer therapeutics. *Cell Res* **17:** 195–211

Gartenberg MR (2000) The Sir proteins of *Saccharomyces cerevisiae*: mediators of transcriptional silencing and much more. *Curr Opin Microbiol* **3:** 132–137

Glaser KB, Li J, Staver MJ, Wei RQ, Albert DH, Davidsen SK (2003) Role of class I and class II histone deacetylases in carcinoma cells using siRNA. *Biochem Biophys Res Commun* **310:** 529–536

Gregoire S, Xiao L, Nie J, Zhang X, Xu M, Li J, Wong J, Seto E, Yang XJ (2007) Histone deacetylase 3 interacts with and deacetylates myocyte enhancer factor 2. *Mol Cell Biol* **27:** 1280–1295

Grignani F, De Matteis S, Nervi C, Tomassoni L, Gelmetti V, Cioce M, Fanelli M, Ruthardt M, Ferrara FF, Zamir I, Seiser C, Grignani F, Lazar MA, Minucci S, Pelicci PG (1998) Fusion proteins of the retinoic acid receptor-alpha recruit histone deacetylase in promyelocytic leukaemia. *Nature* **391:** 815–818

Guan HP, Ishizuka T, Chui PC, Lehrke M, Lazar MA (2005) Corepressors selectively control the transcriptional activity of PPARgamma in adipocytes. *Genes Dev* **19:** 453–461

Guenther MG, Barak O, Lazar MA (2001) The SMRT and N-CoR corepressors are activating cofactors for histone deacetylase 3. *Mol Cell Biol* **21:** 6091–6101

Guidez F, Ivins S, Zhu J, Soderstrom M, Waxman S, Zelent A (1998) Reduced retinoic acid-sensitivities of nuclear receptor corepressor binding to PML- and PLZF-RARalpha underlie molecular pathogenesis and treatment of acute promyelocytic leukemia. *Blood* **91:** 2634–2642

Guidez F, Petrie K, Ford AM, Lu H, Bennett CA, MacGregor A, Hannemann J, Ito Y, Ghysdael J, Greaves M, Wiedemann LM, Zelent A (2000) Recruitment of the nuclear receptor corepressor N-CoR by the TEL moiety of the childhood leukemia-associated TEL-AML1 oncoprotein. *Blood* **96:** 2557–2561

Haga S, Ogawa W, Inoue H, Terui K, Ogino T, Igarashi R, Takeda K, Akira S, Enosawa S, Furukawa H, Todo S, Ozaki M (2005) Compensatory recovery of liver mass by Akt-mediated hepatocellular hypertrophy in liver-specific STAT3-deficient mice. *J Hepatol* **43:** 799–807

Hartman HB, Yu J, Alenghat T, Ishizuka T, Lazar MA (2005) The histone-binding code of nuclear receptor co-repressors matches the substrate specificity of histone deacetylase 3. *EMBO Rep* **6:** 445–451

Hay N, Sonenberg N (2004) Upstream and downstream of mTOR. *Genes Dev* **18:** 1926–1945

He LZ, Guidez F, Tribioli C, Peruzzi D, Ruthardt M, Zelent A, Pandolfi PP (1998) Distinct interactions of PML-RARalpha and PLZF-RARalpha with co-repressors determine differential responses to RA in APL. *Nat Genet* **18:** 126–135

Hernandez R, Teruel T, Lorenzo M (2001) Akt mediates insulin induction of glucose uptake and up-regulation of GLUT4 gene expression in brown adipocytes. *FEBS Lett* **494:** 225–231

Hubbert C, Guardiola A, Shao R, Kawaguchi Y, Ito A, Nixon A, Yoshida M, Wang XF, Yao TP (2002) HDAC6 is a microtubule-associated deacetylase. *Nature* **417:** 455–458

Imai S, Armstrong CM, Kaeberlein M, Guarente L (2000) Transcriptional silencing and longevity protein Sir2 is an NAD-dependent histone deacetylase. *Nature* **403:** 795–800

Jacinto E, Loewith R, Schmidt A, Lin S, Ruegg MA, Hall A, Hall MN (2004) Mammalian TOR complex 2 controls the actin cytoskeleton and is rapamycin insensitive. *Nat Cell Biol* **6:** 1122–1128

Juan LJ, Shia WJ, Chen MH, Yang WM, Seto E, Lin YS, Wu CW (2000) Histone deacetylases specifically down-regulate p53-dependent gene activation. *J Biol Chem* **275:** 20436–20443

Kuhn R, Schwenk F, Aguet M, Rajewsky K (1995) Inducible gene targeting in mice. *Science* **269:** 1427–1429

Lagger G, O'Carroll D, Rembold M, Khier H, Tischler J, Weitzer G, Schuettengruber B, Hauser C, Brunmeir R, Jenuwein T, Seiser C. (2002) Essential function of histone deacetylase 1 in proliferation control and CDK inhibitor repression. *EMBO J* **21:** 2672–2681

Lahm A, Paolini C, Pallaoro M, Nardi MC, Jones P, Neddermann P, Sambucini S, Bottomley MJ, Lo Surdo P, Carfi A, Koch U, De Francesco R, Steinkuhler C, Gallinari P (2007) Unraveling the hidden catalytic activity of vertebrate class IIa histone deacetylases. *Proc Natl Acad Sci USA* **104:** 17335–17340

Lehmann JM, Moore LB, Smith-Oliver TA, Wilkison WO, Willson TM, Kliewer SA (1995) An antidiabetic thiazolidinedione is a high affinity ligand for peroxisome proliferator-activated receptor gamma (PPAR gamma). *J Biol Chem* **270:** 12953–12956

Li J, Wang J, Wang J, Nawaz Z, Liu JM, Qin J, Wong J (2000) Both corepressor proteins SMRT and N-CoR exist in large protein complexes containing HDAC3. *EMBO J* **19:** 4342–4350

Li Y, Kao GD, Garcia BA, Shabanowitz J, Hunt DF, Qin J, Phelan C, Lazar MA (2006) A novel histone deacetylase pathway regulates mitosis by modulating Aurora B kinase activity. *Genes Dev* **20:** 2566–2579

Lin RJ, Nagy L, Inoue S, Shao W, Miller Jr WH, Evans RM (1998) Role of the histone deacetylase complex in acute promyelocytic leukaemia. *Nature* **391:** 811–814

Loewith R, Jacinto E, Wullschleger S, Lorberg A, Crespo JL, Bonenfant D, Oppliger W, Jenoe P, Hall MN (2002) Two TOR complexes, only one of which is rapamycin sensitive, have distinct roles in cell growth control. *Mol Cell* **10:** 457–468

Luo J, Su F, Chen D, Shiloh A, Gu W (2000) Deacetylation of p53 modulates its effect on cell growth and apoptosis. *Nature* **408:** 377–381

Marks PA, Richon VM, Breslow R, Rifkind RA (2001) Histone deacetylase inhibitors as new cancer drugs. *Curr Opin Oncol* **13:** 477–483

Mi H, Guo N, Kejariwal A, Thomas PD (2007) PANTHER version 6: protein sequence and function evolution data with expanded representation of biological pathways. *Nucleic Acids Res* **35:** D247–D252

Mordier S, Iynedjian PB (2007) Activation of mammalian target of rapamycin complex 1 and insulin resistance induced by palmitate in hepatocytes. *Biochem Biophys Res Commun* **362:** 206–211

Ono H, Shimano H, Katagiri H, Yahagi N, Sakoda H, Onishi Y, Anai M, Ogihara T, Fujishiro M, Viana AY, Fukushima Y, Abe M, Shojima N, Kikuchi M, Yamada N, Oka Y, Asano T (2003) Hepatic Akt activation induces marked hypoglycemia, hepatomegaly, and hypertriglyceridemia with sterol regulatory element binding protein involvement. *Diabetes* **52:** 2905–2913

Papeleu P, Loyer P, Vanhaecke T, Elaut G, Geerts A, Guguen-Guillouzo C, Rogiers V (2003) Trichostatin A induces differential cell cycle arrests but does not induce apoptosis in primary cultures of mitogen-stimulated rat hepatocytes. *J Hepatol* **39:** 374–382

Picard F, Kurtev M, Chung N, Topark-Ngarm A, Senawong T, Machado De Oliveira R, Leid M, McBurney MW, Guarente L (2004) Sirt1 promotes fat mobilization in white adipocytes by repressing PPAR-gamma. *Nature* **429:** 771–776

Postic C, Magnuson MA (2000) DNA excision in liver by an albumin-Cre transgene occurs progressively with age. *Genesis* **26:** 149–150

Postic C, Shiota M, Niswender KD, Jetton TL, Chen Y, Moates JM, Shelton KD, Lindner J, Cherrington AD, Magnuson MA (1999) Dual roles for glucokinase in glucose homeostasis as determined by liver and pancreatic beta cell-specific gene knock-outs using Cre recombinase. *J Biol Chem* **274:** 305–315

Ren D, Collingwood TN, Rebar EJ, Wolffe AP, Camp HS (2002) PPARgamma knockdown by engineered transcription factors: exogenous PPARgamma2 but not PPARgamma1 reactivates adipogenesis. *Genes Dev* **16:** 27–32

Santini V, Gozzini A, Ferrari G (2007) Histone deacetylase inhibitors: molecular and biological activity as a premise to clinical application. *Curr Drug Metab* **8:** 383–393

Sanyal AJ (2005) Mechanisms of disease: pathogenesis of nonalcoholic fatty liver disease. *Nat Clin Pract Gastroenterol Hepatol* **2:** 46–53

Shimazu T, Komatsu Y, Nakayama KI, Fukazawa H, Horinouchi S, Yoshida M (2006) Regulation of SV40 large T-antigen stability by reversible acetylation. *Oncogene* **25:** 7391–7400

Takami Y, Nakayama T (2000) N-terminal region, C-terminal region, nuclear export signal, and deacetylation activity of histone deacetylase-3 are essential for the viability of the DT40 chicken B cell line. *J Biol Chem* **275:** 16191–16201

Thomas PD, Campbell MJ, Kejariwal A, Mi H, Karlak B, Daverman R, Diemer K, Muruganujan A, Narechania A (2003) PANTHER: a library of protein families and subfamilies indexed by function. *Genome Res* **13:** 2129–2141

Tontonoz P, Hu E, Spiegelman BM (1994) Stimulation of adipogenesis in fibroblasts by PPAR gamma 2, a lipid-activated transcription factor. *Cell* **79:** 1147–1156

Trivedi CM, Luo Y, Yin Z, Zhang M, Zhu W, Wang T, Floss T, Goettlicher M, Noppinger PR, Wurst W, Ferrari VA, Abrams CS, Gruber PJ, Epstein JA (2007) Hdac2 regulates the cardiac hypertrophic response by modulating Gsk3 beta activity. *Nat Med* **13:** 324–331

Wang L, Hiebert SW (2001) TEL contacts multiple co-repressors and specifically associates with histone deacetylase-3. *Oncogene* **20:** 3716–3725

Werman A, Hollenberg A, Solanes G, Bjorbaek C, Vidal-Puig AJ, Flier JS (1997) Ligand-independent activation domain in the N terminus of peroxisome proliferator-activated receptor gamma (PPARgamma). Differential activity of PPARgamma1 and -2 isoforms and influence of insulin. *J Biol Chem* **272:** 20230–20235

Widmer J, Fassihi KS, Schlichter SC, Wheeler KS, Crute BE, King N, Nutile-McMenemy N, Noll WW, Daniel S, Ha J, Kim KH, Witters LA (1996) Identification of a second human acetyl-CoA carboxylase gene. *Biochem J* **316** (Part 3)**:** 915–922

Xu F, Rychnovsky SD, Belani JD, Hobbs HH, Cohen JC, Rawson RB (2005) Dual roles for cholesterol in mammalian cells. *Proc Natl Acad Sci USA* **102:** 14551–14556

Yoon HG, Chan DW, Huang ZQ, Li J, Fondell JD, Qin J, Wong J (2003) Purification and functional characterization of the human N-CoR complex: the roles of HDAC3, TBL1 and TBLR1. *EMBO J* **22:** 1336–1346

Yu S, Matsusue K, Kashireddy P, Cao WQ, Yeldandi V, Yeldandi AV, Rao MS, Gonzalez FJ, Reddy JK (2003) Adipocyte-specific gene expression and adipogenic steatosis in the mouse liver due to peroxisome proliferator-activated receptor gamma1 (PPARgamma1) overexpression. *J Biol Chem* **278:** 498–505

Zhang YL, Hernandez-Ono A, Siri P, Weisberg S, Conlon D, Graham MJ, Crooke RM, Huang LS, Ginsberg HN (2006) Aberrant hepatic expression of PPARgamma2 stimulates hepatic lipogenesis in a mouse model of obesity, insulin resistance, dyslipidemia, and hepatic steatosis. *J Biol Chem* **281:** 37603–37615

Zhu MY, Hasty AH, Harris C, Linton MF, Fazio S, Swift LL (2005) Physiological relevance of apolipoprotein E recycling: studies in primary mouse hepatocytes. *Metabolism* **54:** 1309–1315

Zhu Y, Alvares K, Huang Q, Rao MS, Reddy JK (1993) Cloning of a new member of the peroxisome proliferator-activated receptor gene family from mouse liver. *J Biol Chem* **268:** 26817–26820

Zupkovitz G, Tischler J, Posch M, Sadzak I, Ramsauer K, Egger G, Grausenburger R, Schweifer N, Chiocca S, Decker T, Seiser C (2006) Negative and positive regulation of gene expression by mouse histone deacetylase 1. *Mol Cell Biol* **26:** 7913–7928

